Experimental determination of pressure coefficients for flood loading of walls of Dutch terraced houses

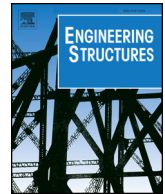Jansen, L.; Korswagen , P.A.; Bricker, J.D.; Pasterkamp, S.; de Bruijn, K.M.; Jonkman, S.N.

Important note
To cite this publication, please use the final published version (if applicable).
Please check the document version above.

Experimental determination of pressure coefficients for flood loading of walls of Dutch terraced houses

L. Jansen[a], P.A. Korswagen[a,b,*], J.D. Bricker[a,c,e], S. Pasterkamp[a,b], K.M. de Bruijn[d], S.N. Jonkman[a,c]

[a] Faculty of Civil Engineering and Geosciences, Delft University of Technology, Stevinweg 1, 2628 CN Delft, The Netherlands
[b] Department of Materials, Mechanics, Management & Design
[c] Department of Hydraulic Engineering
[d] Deltares, Department of Flood Risk Management, Boussinesqweg 1, 2600 MH Delft, The Netherlands
[e] Department of Civil and Environmental Engineering, University of Michigan, 2350 Hayward Street, Ann Arbor MI 48109-2125, USA

ABSTRACT

Failure of residential buildings during floods is an important cause of damage and loss of life. In the case of the Netherlands, the collapse of buildings is implicitly included in current damage and mortality curves since these are generated from historical data. However, the Netherlands has not experienced destructive flooding since 1953, so damage functions for modern buildings do not exist. Therefore, this paper assesses the effect of floods on modern Dutch residences with laboratory tests and structural models in order to formulate physically-based fragility curves. The results gathered are also applicable to similarly-built masonry and cavity-wall rowhouses elsewhere.

Almost half of the Dutch population live in terraced houses (also known as townhouses or rowhouses), of which the critical failure mechanism during a flood is out-of-plane bending of the load-bearing walls. Failure of these structural elements should be analysed with the pressure coefficient, C_p, instead of the currently used drag coefficient, C_D, because wall collapse is more likely than displacement of the entire structure. This paper describes the quantification of both coefficients by conducting flume experiments on rectangular boxes with different geometries and orientations. Higher drag coefficients are derived from the experiments than provided by FEMA, resulting in higher hydrodynamic loads on the residences.

The physical approach to evaluate the collapse of residences is exemplified with a case study of the three most common type of residences in the Netherlands. Structural analyses of their load-bearing walls subjected to a hydrostatic and hydrodynamic load perpendicular to the wall show failure due to milder flood conditions than the current damage curves do for all case study residences. A sensitivity analysis shows an important influence of wall thickness, initial axial loading of the wall, and the flood water level inside the residence.

1. Introduction

Flood fatality plays an important role in flood risk management decisions. The new flood protection standards in the Netherlands for example, were based on, amongst others, the individual flood risk and societal risk, both of which are fatality risks. Also, in France, the UK, and the USA there is an increasing attention to the risk of loss of life. To assess mortality and potential fatality numbers, mortality functions are used which provide mortality as a function of flood characteristics such as water depth, flow velocity and the rate of water level rise [22]. An important contributor to the risk of fatality is the degree of survivability inside and around structures, especially when evacuation is difficult; for

example, the collapse of buildings caused most fatalities during the 1953 storm surge disaster in The Netherlands, also known as the "Watersnoodramp" [23]. The aforementioned flood was so catastrophic that it triggered the so-called 'Deltaworks' in the Netherlands, comprising the renovation and construction of new dikes, dams, (moveable) barriers, and gates, which have prevented such a flood from occurring since. Other comparatively smaller floods, like the river floods of 1993–1995 in the east of the Netherlands [40], did not lead to severe building damage. Yet, recent floods like those caused by the storms Dennis in the UK and Xynthia in France in 2010 do highlight the importance of building behaviour during floods.

The existing mortality functions, paramount for understanding flood

risk, have thus been developed by analysing empirical information from historical floods between 1934 and 1965 [8,14]. Changes in construction techniques over the years have made these functions outdated. Currently, a correction factor is proposed to consider the change of building quality due to new building regulations and development of knowledge, materials and construction techniques [3], but its calibration remains uncertain. Consequently, this paper proposes to assess building collapse with an approach alternative to that of the empirical functions, namely, a physical evaluation for the purpose of quantifying flood fatality and risk.

Furthermore, the available damage functions obtained from empirical studies show a large scatter due to the inclusion of different types of residences, and an upper value is given by Clausen and Clark [1] for masonry and concrete residences in the form of a critical depth velocity product [m²/s]. The latter function is still used, but the correlation between the flood characteristics and the damage observation is empirical and unclear, and is dependent on building characteristics according to multiple studies, see Pistrika and Jonkman [17]. A physical approach tacked to specific building (sub)typologies should reduce this scatter and provide more targeted results.

This paper aims thus to contribute to the improvement of damage and mortality functions by reassessing the loads on rectangular buildings. A physical approach is adopted to determine which flood conditions cause structural damage to the residential structures in the current building stock. Since building collapse was a dominant cause of fatalities as stated, knowledge of improved building strength will then contribute to improved building fragility functions, and so to mortality functions.

Flooding of an urban area causes different actions on a building; an overview is given by Kelman and Spence [10]. The current Dutch mortality functions, as well as many other existing damage functions, are dependent on the water depth, h, and flow velocity, v. Therefore, the hydrostatic load, $q_H = \rho \cdot g \cdot h$, where '$\rho$' is the density of water and 'g' the gravitational acceleration, and quasi-steady component of the hydrodynamic load, $q_D = \frac{1}{2} \cdot C_D \cdot \rho \cdot v^2$, where '$C_D$' is the drag coefficient, are considered to be the most important actions for the collapse of residences. Other flood actions like scour, buoyancy and non-physical actions are expected to cause damage, but not immediate collapse. The impact of debris, on the other hand, is an influential load often causing great damage to structures [41]; however, it does not affect all structures and is also unlikely to occur in Dutch flooding scenarios [23]. Hence, it will be neglected in this study. If debris were considered, its magnitude would likely overpower most of the refinements proposed herein [42]. Furthermore, the flood infiltration rate, or, how fast water will enter a structure, is also uncertain. Consequently, the most critical loading situation (without debris) is taken into consideration in this paper by using a quick rise rate resulting in no water inside the residence as pictured in Fig. 1.

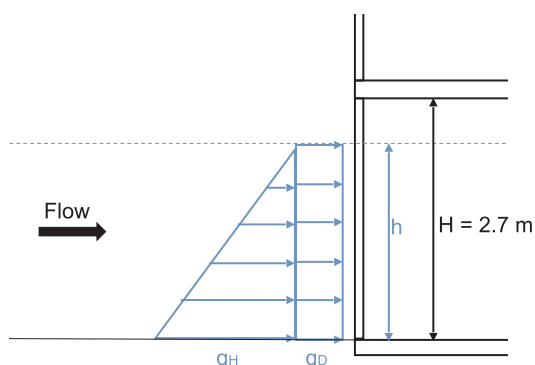In the case of a bluff object (i.e. an object with sharp edges which is not streamlined) subjected to moving water, the drag coefficient, C_D, mainly depends on the shape of the object. Furthermore, the vertical blockage of the flood water due to the building (an emerged object) also influences the drag coefficient, which is included in the Coastal Construction Manual as the aspect ratio, B/h [4], herein denoted the width/waterdepth aspect ratio. However, due to the difference in geometry of the residences in the Netherlands (terraced houses with an elongated rectangular footprint) and the USA (detached houses with a nearly square footprint), these drag coefficients cannot be adopted directly. A similar loading is observed for buildings subjected to wind and comparable coefficients from multiple wind-tunnel studies for objects subjected to both moving air and water can be derived [16].

When observing wind loading, the pressure coefficient (which differs per side of the object), C_p, is used instead of a single drag coefficient, C_D, which defines the net load on the object as a whole and as if it were a solid body. For example, according to the EuroCode, the wind pressure per face of the building can be obtained by multiplying the peak velocity pressure, $q_p = \frac{1}{2} \cdot \rho_{air} \cdot u^2$, where 'u' is the regional wind speed and 'ρ_{air}' is the density of air, with a force coefficient, c_f (EN 1991–1-4), which gives a similar equation as that used for the quasi-steady component of the hydrodynamic load. Buildings consisting of multiple structural elements do not necessarily behave as stiff objects, in contrast to the piers of bridges or other objects in hydraulic engineering. Therefore, pressure coefficients should be used by assessing the resistance of a single element in a residence subjected to a certain combination of water depth and flow velocity, as is done for wind loads, instead of employing drag coefficients. Drag coefficients are important when assessing the flood effect at the foundation level, but failure of masonry residences is characterised by failure of individual walls; moreover, analyses of the walls are more reliable when evaluating the pressure on them and not the drag on the entire structure. Furthermore, while hydrostatic pressure is well understood, the hydrodynamic pressure, affected by the characteristics of the flood flow, requires additional insight. It must be noted, also, that the approach of distinguishing between hydrostatic and hydrodynamic pressure is only reasonable as long as the flow remains quasi-steady; for highly unsteady flows like bore impact, a general pressure or force coefficient would be more convenient [35–37]. Nonetheless, the Dutch flooding characteristics are such that the quasi-steady approach is applicable and thus, the analysis of structures with a pressure coefficient for individual components offers higher precision and lower uncertainty.

In order to define the pressure coefficients dependent on the geometry of the building compared to the water depth, both the expected water depth and the dimensions of typical Dutch residences are necessary. The residences of interest are located in areas prone to flooding as a result of the failure of primary and/or regional flood defences or in the unprotected areas outside the levees [19].

In practice, flood mortality functions employ the depth and velocity output by large-scale flood models; these models are incapable of resolving the precise depth and velocity at the local scale considering individual buildings and streets [14]; hence, the pressure coefficient which this study aims to determine is not related to the local flow characteristics, but to the general flood parameters as determined by bare-earth flood models using equivalent roughness values to represent buildings. Consequently, the changes occurring at the local scale due to the presence of houses and other obstacles to the flow, are to be included and parametrised in the pressure coefficient and considered to be the hydrodynamic effect. This approach is similar to that of wind loading, where the regional expected wind speed is used for design and individual pressure coefficients are applied to evaluate various structural elements.

In Fig. 2, a typical terraced house (in Dutch: rijtjeshuis) is shown. About half of the Dutch live in such residences, which are similar throughout the country's flood-prone areas [7]. Most were built between 1965 and 1994 with a common width of 5.4 m due to the use of precast concrete filigree slabs for floors (in Dutch: breedplaatvloer) and hollow core slab floors from the 1970s onwards.

Fig. 1. Considered flood actions on wall.

Fig. 2. Row of terraced houses.

The paper begins with the methodology of quantifying the pressure coefficients, starting with the flood models used to generate the expected flood characteristics. Next, the set-up of the physical model and the various experiments conducted are described (section 2). Subsequently in section 3, the water level, velocity and pressure profiles from which the coefficients are determined are shown. The differences between the experiments are elaborated, complemented by comparisons with values from the literature in this introduction. Finally, the resistance of the terraced houses subjected to the Dutch flood conditions is explored in section 4 by using the newly obtained coefficients to analyse three case studies.

2. Material and methods

2.1. General

Spatial flood characteristics are typically generated from a simulation of a flood hazard in a hydraulic model using land-use maps to define the appropriate roughness per cell, where urban areas are generally modelled as flat areas with a high roughness [19]. To analyse if residences collapse due to this hazard, the flood characteristics at the location of the building are needed. However, the global flood characteristics inside these areas with high urbanisation rates are not adequate to assess individual structures [17,25], so higher resolution hydrodynamic models are now under development to better define the

local flood characteristics. The framework pictured in Fig. 3 describes the translation of the flood characteristics from the hazard maps to the actual load due to flooding on the buildings.

In this study, the local flood load (at the building) is quantified by conducting laboratory flume experiments with a timber box schematised in Fig. 4, which represents a row of four typical Dutch terraced houses. When an obstacle, such as the timber box, is placed in the flume, stagnant flow in the longitudinal direction occurs just in front of the frontal face of the building and water is pushed up altering the flow. Therefore, prior to these experiments, the free-stream characteristics are captured during the baseline experiments at the location of the front face of the building (Fig. 3 top right). This water depth and flow velocity measured without the box being present can be compared with the global flood characteristics from hazard maps generated from the hydraulic flood model (Fig. 3 top left). Hence, the drag and pressure coefficients can be determined from the pressures measured during the laboratory flood experiments (Fig. 3 bottom right). If the newer models are able to generate reliable local flood characteristics (Fig. 3 bottom left), these could be transferred directly to local flood characteristics in the experiments to measure the pressures on the buildings.

2.2. Experimental set-up

The experiments were conducted with a physical model (scale 1:50) in the Fluid Mechanics Laboratory of the Department of Hydraulic Engineering at the Delft University of Technology (Fig. 4). The Wave Overtopping Simulator [18] was used to generate a typical dam-break wave; the steel gate was lifted when the water depth in the reservoir reached the desired impoundment depth to enable water to flow into the prismatic flume. The formation and propagation of the dynamic wave and free-falling movement of the water near the free surface are uninfluenced by the gate due to its short opening time of 0.13–0.20 s for impoundment depths of 105 to 210 mm [12,27,28]. The volume of water in the reservoir was around 100L. Due to the reduced scale of the experiments, it is necessary to briefly discuss potential scale effects. The experiment was designed such that the Froude number (inertia - gravity) was comparable between the reduced scale and the true scale. Additionally, other dimensionless numbers were set well above the critical values [38] of 120 for the Weber number (inertia - capillary force, with a minimum of 500 during the quasi-steady part) and 2000 for the Reynolds number (inertia - viscosity, with a minimum of 25,000 during the experiments). Nonetheless, the high Cauchy number (force – elastic force) will result in an interaction with the structure which will behave too stiffly in comparison with a real structure, since the
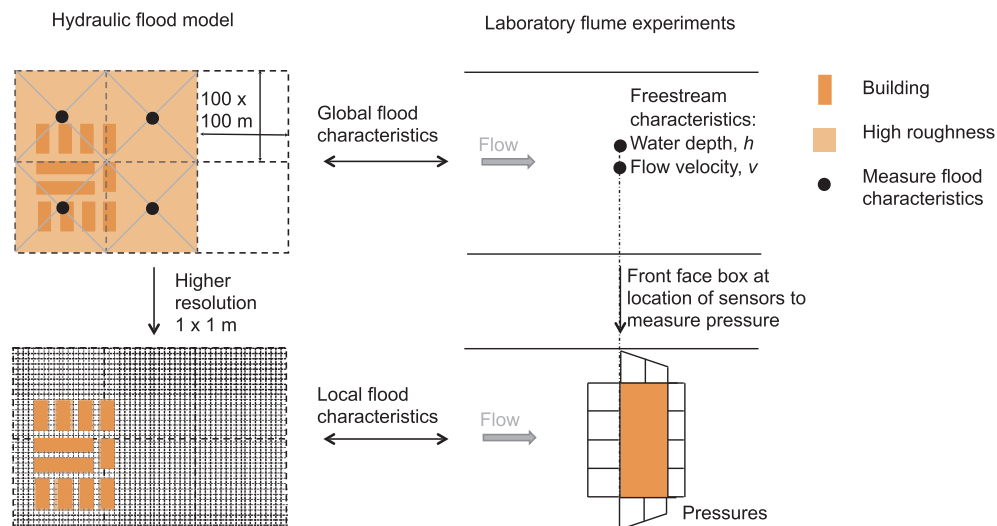

Fig. 3. Translation of flood characteristics between models (all illustrations are plan views).
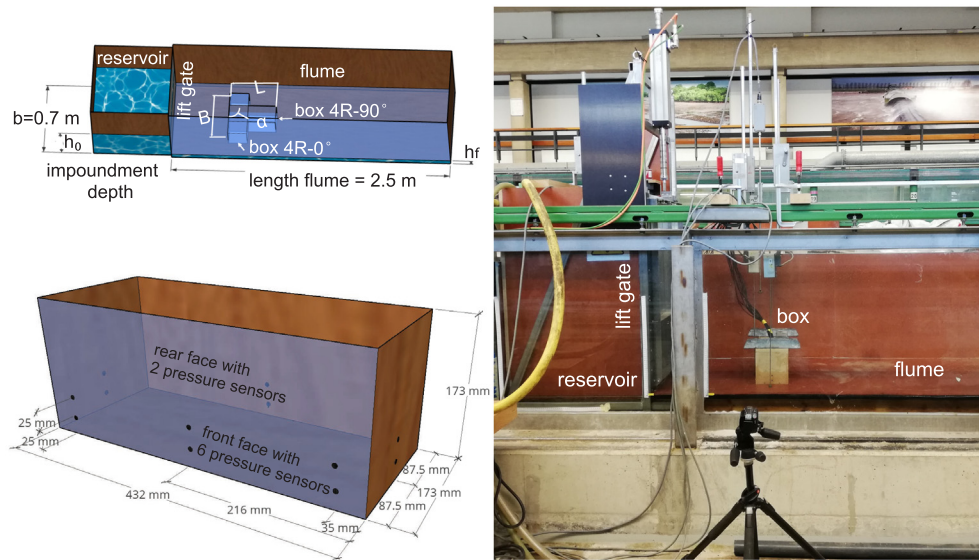
Fig. 4. Experimental set-up at TU Delft.

elasticity of a house couldn't be scaled with the experimental box. Moreover, the influence of the atmospheric pressure (Euler number) would be too large as well. Both of these two last effects will result in a slight over-prediction of the impact pressures, making the experimental model conservative when compared to the true scale. However, for quasi-static loads this is not an issue.

The free-stream characteristics of the incoming wave were captured for three impoundment depths during the baseline experiments by placing a wave gauge and an electromagnetic velocity sensor (EMS) at the location where the centreline of the front face of the building will be in later experiments. To assume the measured velocity to be uniform over the water depth, both the elevation of the EMS above the bed of the flume and the initial water depth in the flume, h_f, were approximately 15 mm [31]. Subsequent to the baseline experiments, the pressures due to these dam-break waves were measured by twelve pressure sensors integrated into the four vertical faces of the box. The pressure at different locations on the various faces of the box was measured, see Fig. 4; the resultant force was not measured but is later computed from these pressure sensors. Note also that the distance between the gate and the obstacle was 0.5 m meters, which was insufficient for the bore to fully develop when reaching the box. Since there was always an initial water level in the flume, the bore developed on a wet bed. Additionally, the maximum waterdepth of the so-called plateau was also not reached. However, since the quasi-steady state, which was needed to determine the pressure coefficients, was achieved, the experiment was deemed effective.

To investigate the influence of both the geometry of the box compared to the water depth and the orientation of the box compared to the flow direction, 18 different configurations of the experiments were performed and are summed up in Table 1 and explained in Fig. 5. To work with comparable side-ratios (length, L, over width, B) as given in literature, a length of an individual residence of 8.64 m is chosen related to the scaling up of useful dimensions for the flume, which is within the common length range of 8.5–9.8 m [24]. Rows of four
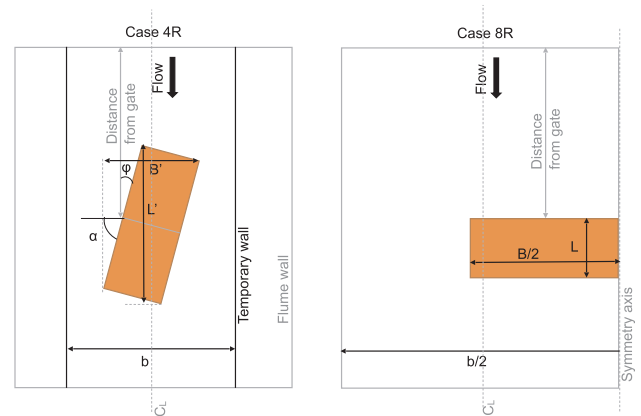
residences form bodies of 21.6 by 8.64 m, leading to a side-ratio of 2.5 or 0.4 depending on the orientation of the body compared to the flow. For all configurations, the ratio of the projected width of the box, B', to the width of the flow, b, i.e. the blockage ratio, B'/b, is kept between 0.53 and 0.57 by placing temporary walls in the flume to narrow the width of the flow to minimise the influence of this parameter on the determination of the coefficient.

The influence of twice as many residences in a row (i.e. eight instead of four; 8R instead of 4R) is investigated by considering one side of the flume as the symmetry axis and placing the box with its shortest face to this side. Since the flow is uniform over the width of the flume, the flow pattern is identical on both sides of the box resulting in a symmetry-axis through the centreline of the box parallel to the length of the flume. The configuration of the box placed with its longest face perpendicular to the flow direction is referred to as a rotation, α, of 0°, resulting in an angle of attack or flow incidence, φ, of 90° on the frontal

Fig. 5. Configuration of the box.

Table 1
Configurations of the experiments. 4R indicates a rowhouse equal to the length of 4 individual houses, and 8R indicates a rowhouse equal to the length of 8 individual houses.

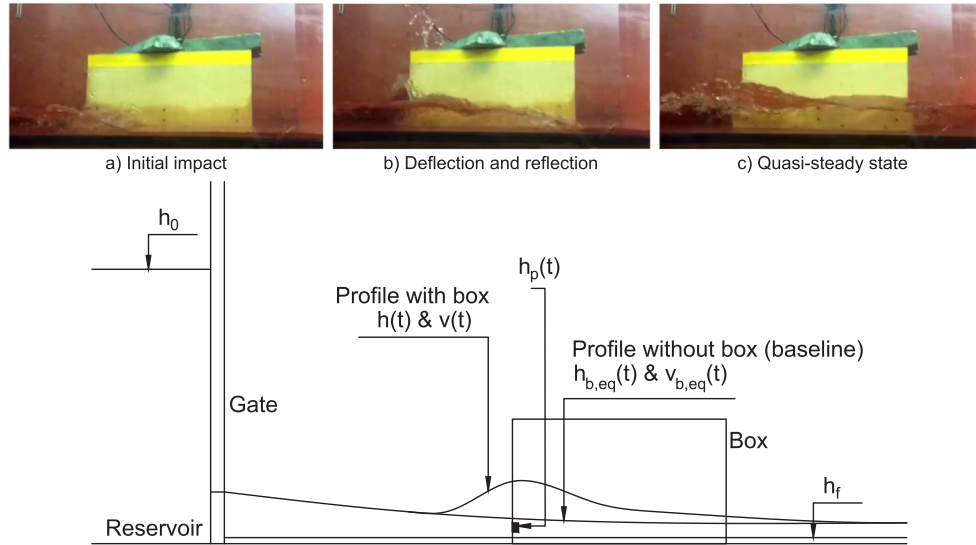| Case	Width, B [mm]	Length, L [mm]	Rotation, α [°]	Impoundment depth, h_0 [mm]
4R	432	173	0, 15, 45, 75, 90	150, 175, 200
8R	864	173	0	150, 175, 200

Fig. 6. Snapshot of the experiment (h_0 = 175 mm, α = 75°) and schematisation of variables. Note that the scale and profiles are only exemplifying.

face, see Fig. 5. By rotating the box by a certain angle, this angle of attack on the frontal face decreases while the angle on the side face increases. The distance between the centreline of the longest face and the gate remains constant for all orientations except for the rotation of 90°, where this constant distance is enforced between the shortest face and the gate.

2.3. Determination of the drag and pressure coefficients

The coefficients can be derived from the face pressure on the box caused by the flow velocity. The equivalent baseline water depth is subtracted from the measured pressure on the box, expressed in the water depth, $h_p(t)$, to obtain the pressure due to the quasi-steady hydrodynamic load effect, Δh. Measuring of the actual water depth, $h(t)$, during the box-experiments would be inaccurate due to splashes and a tongue of water hitting the wave gauge. This effect can be seen in snapshots on one of the experiments; see Fig. 6. Note that throughout this text, only the hydrodynamic pressure is discussed, since the hydrostatic load does not affect pressure or drag coefficients in the quasi-steady state.

Nonetheless, minor differences in the impoundment depth, h_0 or $h_{b,0}$ (for baseline experiments), and the initial water depth in the flume, h_f or $h_{b,f}$, between the baseline experiments and experiments with the box are observed; see Fig. 4 for notation. To take these differences into account, the free-stream water depth and flow velocity are normalised by making these parameters independent of the initial conditions. These dimensionless values, $h_n(t)$ and $v_n(t)$, only dependent on time, are later used to calculate the equivalent water depth, $h_{b,eq}(t)$, and equivalent flow velocity, $v_{b,eq}(t)$, from the baseline experiments using the initial conditions of the experiments with the box and thus become the free-stream flow characteristics for comparison. From these baseline characteristics and the measured pressure, the pressure coefficient, C_p, can be derived. A summary of the process is presented next:

Experiments for the baseline cases without the box, are conducted, $h_{b,f}$ and $h_{b,0}$ are measured before opening the gate. Then, $h_b(t)$ and $v_b(t)$ are measured in the flume at the position where the box will be. For each impoundment depth, $h_{b,0}$, five runs are performed; see later Table 2.
Normalised values of water depth, h_n, and of velocity, v_n, both functions of time and independent of the exact initial conditions, are computed from the baseline experiments; see Eq. (1).

$$\left. \begin{aligned} h_n(t) &= \frac{h_b(t) - h_{b,f}}{h_{b,0} - h_{b,f}} \\ v_n(t) &= \frac{v_b(t)}{\sqrt{g \cdot (h_{b,0} - h_{b,f})}} \end{aligned} \right\} \tag{1}$$

The box with pressure sensors is placed in the flume; h_f and h_0 are measured.
The gate is opened and pressures are measured on the faces of the box (h_p). Waterdepth or velocity values, measured during the experiments with the box, are not used for the determination of C_p.
The equivalent baseline waterdepth and velocity, $h_{b,eq}$ and $v_{b,eq}$, are calculated using the initial conditions of the experiments with the box (h_f and h_0) and the normalised values from the baseline cases (h_n and v_n); see equation (2).

$$\left. \begin{aligned} h_{b,eq}(t) &= h_n(t) \cdot (h_0 - h_f) + h_f \\ v_{b,eq}(t) &= v_n(t) \cdot \sqrt{g \cdot (h_0 - h_f)} \end{aligned} \right\} \tag{2}$$

The pressure due to the dynamic effect, Δh, is computed by subtracting the baseline waterdepth from the pressure measured by the obstacle's sensors; see Eq. (3).

$$\Delta h(t) = h_p(t) - h_{b,eq}(t) \tag{3}$$

This dynamic pressure, Δh, is used to compute the pressure coefficient, C_p via equation (4).

$$C_p(t) = \frac{\rho \cdot g \cdot \Delta h(t)}{\frac{1}{2}\rho \cdot v_{b,eq}(t)^2} \tag{4}$$

The pressure coefficient is then a parametrisation from the baseline flow taking into account the presence of the obstacle, its orientation towards the flow and the blockage ratio in the flume.
Finally, the drag coefficient can be calculated. While the measured pressures are acting perpendicularly to the face, the drag is working in the direction of the flow as pictured in Fig. 7. To derive the drag coefficient, the integral of the components of the pressure coefficient aligned with the flow direction over the face are summed up as in Equation (5).

$$C_D = \frac{1}{B}(B\cos\alpha \cdot C_{p,front} - L\sin\alpha \cdot C_{p,left} - B\cos\alpha \cdot C_{p,rear} + L\sin\alpha \cdot C_{p,right}) \tag{5}$$

Table 2
Time-averaged values over the quasi-steady interval from the baseline measurements based on 5 runs each (coefficient of variation between brackets).

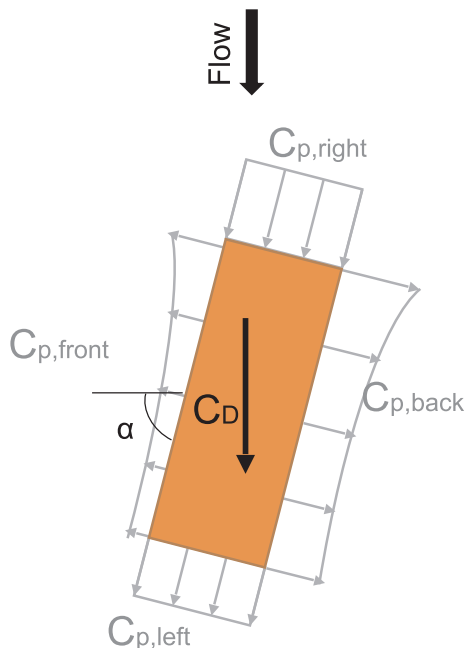| h_0 [mm]	h_n [−]	$h_{b,eq}$ [mm]	$h_{full\ scale}$ [m]	v_n [−]	$v_{b,eq}$ [m/s]	$v_{full\ scale}$ [m/s]
150	0.28	53.1 (0.02)	2.65	0.89	1.01 (0.01)	7.24
175	0.27	58.8 (0.02)	2.94	0.90	1.12 (0.01)	8.13
200	0.26	64.8 (0.07)	3.24	0.93	1.23 (0.03)	8.84

Fig. 7. Definition of pressure and drag coefficient.

3. Experimental results and discussion

3.1. General results

From the baseline experiments, the average of the flow velocity in Fig. 8a and the water depth in Fig. 8b are calculated from five runs per impoundment depth. The water depth inside the reservoir decreases following the analytical dam break solution [20] resulting in a relatively constant water depth at the location of the box between 0.7 and 1.1 s after opening of the gate. During this interval, both the water depth and flow velocity show nearly constant values, with time-averaged values and corresponding coefficients of variation presented in Table 2. Fig. 8c shows the pressure measured by the sensors in the front face of the box and the water depth recorded by the wave gauge just in front of these sensors.

The pressure profiles in Fig. 8c show the characteristic 'church-roof' shape due to different stages in the process of a bore colliding into a building [2], also pictured in Fig. 6. When the bore runs into the building (Fig. 6a), the impulsive load results in a sharp peak in the pressure profile at the frontal face. This initial impact is observed in case of a tsunami [5] or dam-break but is not taken into consideration for the Dutch flooding situation since this is rarely observed for the inundation flow of a polder. After the initial peak, the water depth rises quickly while part of the flow is deflected upwards (i.e. splash-up) and reflected back upstream (Fig. 6b). During this stage, the measured water depth is higher than the measured pressure (expressed in depth units via the hydrostatic approximation) due to these splashes and a thin tongue of water forming on the front face. Subsequently, the quasi-steady state is developed (Fig. 6c) resulting in a smaller second peak in
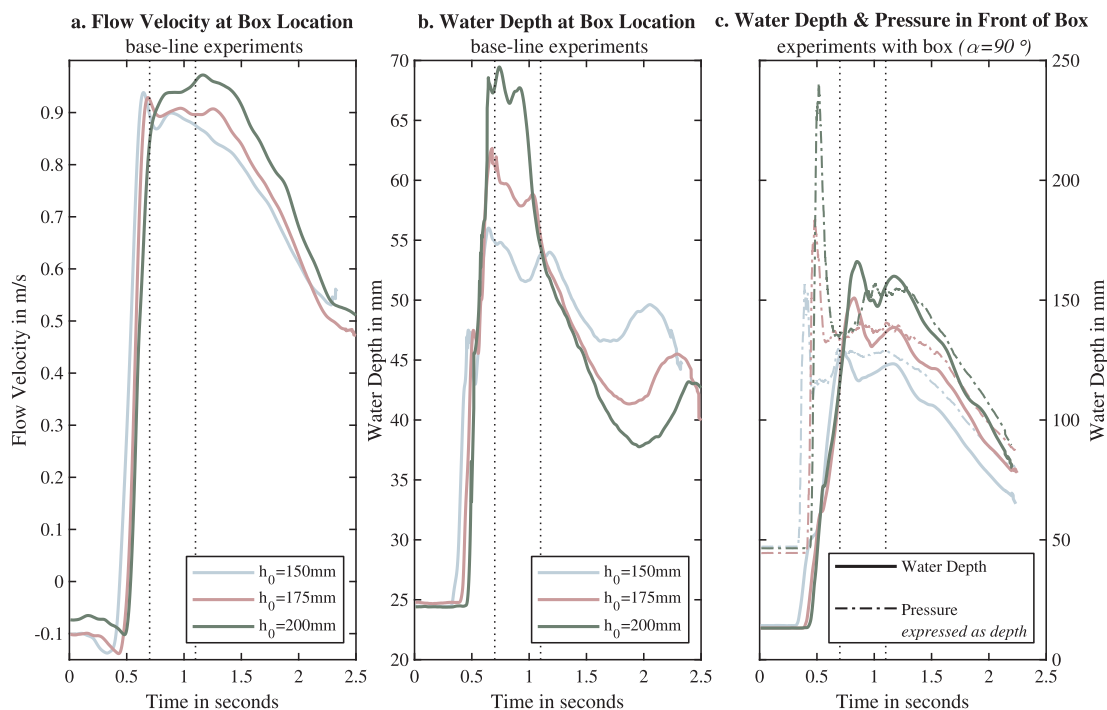

Fig. 8. Mean flow velocity, water depth and measured pressure (expressed in depth units via the hydrostatic approximation) from 5 runs per impoundment depth.

the pressure profile with a longer duration. This is the point from which the coefficients are determined and lies between the dashed vertical lines in Fig. 8.

Similar to the occurrence of the peak load, the quasi-steady load also appears to occur earlier for lower impoundment depths as the maximum water depth is also reached earlier; see Fig. 8c. This delay is not taken into account in this paper, resulting in a slightly higher coefficient of variation of the time-averaged values for the highest impoundment depth in Table 2. Moreover, the values of the water depth measured at the front of the box are comparable to the pressures measured by the sensors in the front face during this quasi-steady flow regime. If the resolution of the local flood characteristics from the hydraulic flood model is fine enough to include the buildings themselves (see Fig. 3), simulated water depths could be transferred easily as a pressure on a certain element of the building, since this is equal to the hydrostatic water pressure due to this water depth. Nonetheless, using the current models with a lower resolution, the flow velocity should be taken into account to determine the pressure on the residence with the help of coefficients.

3.2. Drag and pressure coefficients

The drag coefficients are derived from the combination between the positive pressure at the front face and negative pressure at the rear face as pictured in Fig. 7. Since these pressures are both in the direction of the flow, the drag coefficient in Fig. 9 is, for all configurations, higher than the pressure coefficient on the front face only. Since the aspect-ratio (h/L ratio) remains unchanged when the number of residences is doubled from four to eight, EN 1991-1-4 provides identical pressure coefficients for wind loads for 4R-0° and 8R. For the rear side, the coefficients are approximately equal for both configurations, but for the front side, these were measured to be considerably higher for configuration 8R. This is in line with the increasing drag coefficients provided in P-55, Coastal Construction Manual for increasing B/h ratios [4]. However, due to the difference in geometry of the residences in the Netherlands and the USA these drag coefficients cannot be adopted directly to terraced houses. Nonetheless, the drag coefficients from P-55 [4] are closer to the derived pressure coefficients than the derived drag coefficients from the current experiments as shown in Fig. 9, especially for low side-ratios (L/B). Consequently, if the provided drag coefficients are used for overall stability checks, such as sliding or overturning, an underestimation of the hydrodynamic actions on most rectangular case-study buildings is made.

The derived values for the drag coefficients are lower than those found by others [15,16] in wind-tunnel experiments as pictured in Fig. 10. This can be explained by the small h/L-ratios from the current experiments resulting in smaller negative pressures at the rear face

compared to the high aspect-ratios for taller buildings subjected to wind. On the contrary, the positive pressures on the front face are larger due to the blockage effect in both the width and height, where the vertical blockage of a submerged object is negligible in comparison to the horizontal blockage, whereas this is not the case for wind loading of a building.

Furthermore, an additional comparison can be made against the drag coefficients obtained by Shafiei et al. [39], who experimented with tsunami-like bores in a laboratory flume. They placed a square-shape obstacle in a flume three times as wide as the obstacle and released a bore numerous times while modifying the angle of attack. They obtained slightly higher values than the present study by about 25% and 10%, for angles of 0° and 45°, respectively. These higher values are encouraging given that Shafiei et al. focused on the impact forces of the bore, while this study has put emphasis on the quasi-steady part of the response.

3.3. Influence of city-layout

Looking at the layout of a city, the residences are oriented differently, so the angle of attack and blockage also differ per street or block. The horizontal blockage (at full scale) used in the experiments is comparable to the width of a bicycle path (~3.5 m) for the rotation of 90° and an access road for car drivers, cyclists and pedestrians (~9 m) on both sides of the building for the rotation of 0°. Wider streets result in a smaller blockage ratio, which reduces the pressure on the residences.

Furthermore, the influence of the orientation of the residence compared to the flow is investigated by rotating the building around the centreline of its frontal face pictured in Fig. 5. This rotation, α, changes the angle of attack, φ, or flow incidence on the face of the building. Where a similar minimum of the drag coefficient around a rotation of 75° is found as in the literature in Fig. 10b [16], the pressure coefficients do not show this minimum: an increase of the angle of attack on the face of the building, causes an increase in the pressure coefficient on this face as well.

To summarise, where in a city one row of terraced houses will be subjected to the load from a critical angle of attack of 90°, others will experience lower loads due to a smaller angle of attack without taking the blockage ratio into account. Physical experiments with variations in both the orientations and blockage ratios can be used to find the combined influence of these geometric parameters on the pressure coefficients. The use of higher resolution flood models would enable combining the actual flood characteristics and geometric parameters to define the pressures on the individual residential structures in a city.
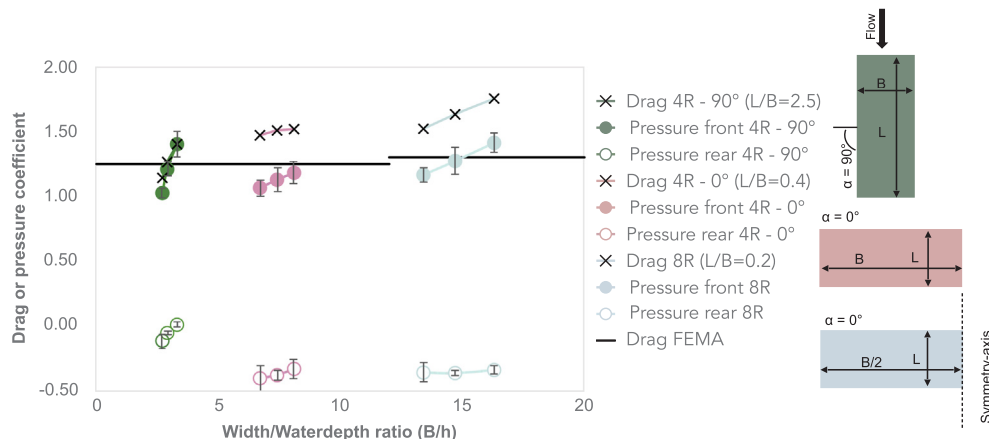

Fig. 9. Influence of the width/depth and geometry aspect ratios on the drag and pressure coefficients.
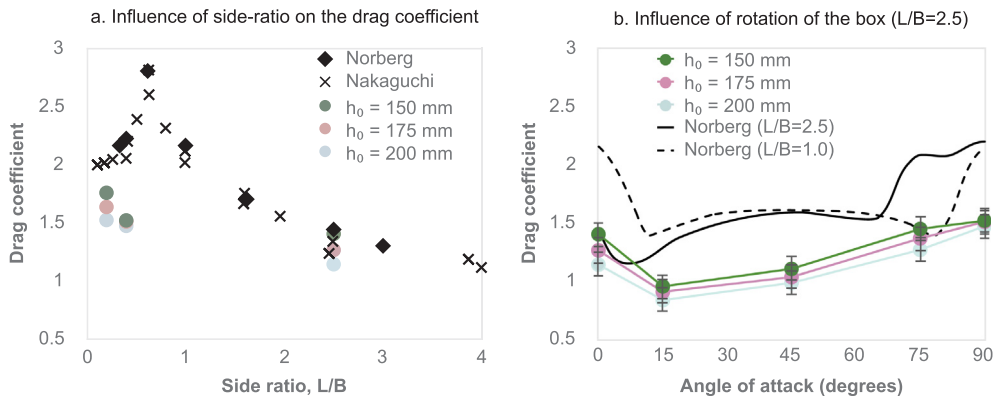
Fig. 10. Comparison of drag coefficients with wind tunnel tests from the literature [1615]

4. Structural analysis of load-bearing walls as case-study

4.1. Introduction of the case-study

To evaluate the capacity of the load-bearing walls of a terraced house, the experimentally determined coefficients are used to define the hydrodynamic loads due to flooding. The majority of the terraced houses consist of two floors with a story-height of 2.7 m and a gable roof construction carried by the party walls which separate the residences from each other; a plan view is depicted in Fig. 11. Due to technical innovations, different building methods, and materials used throughout the years, the typical residences can be roughly divided in residences constructed traditionally with unreinforced masonry (URM) walls containing clay or calcium silicate bricks, and those built with both walls and floors of cast in-situ concrete (in Dutch: gietbouw). Although most of these structural walls are usually cavity walls as illustrated in Fig. 12, only the inner leaf is bearing the upper structure, while the outer leaf is self-supporting and connected to the inner leaf with wall ties.

The residence is likely to collapse if one of the key structural elements fails, such as the foundation, load-bearing walls or other elements which provide stability. Erosion scour can cause instability of shallow foundations, but the flow velocities expected in the Netherlands only exceed the critical value for erosion in very limited areas [21]. In addition, most modern Dutch residences have pile-foundations, which are far less vulnerable to scour than shallow foundations. Consequently, scour is assumed to not be the critical failure mechanism. Stability is provided by the piers in the façade acting as shear elements in the case of the traditionally-built residences shown in Fig. 11 or by the rigid connections between the walls and floors in the case of the concrete residences. Furthermore, since the water depth is seen to equalise quickly on all sides of the row-houses in the experiment, the net lateral load is only due to the hydrodynamic component. The individual load-bearing wall perpendicular to the flow will fail before the overall stability becomes a problem [7]. In sum, it is the out-of-plane bending of the load-bearing inner leaf which is assumed to be the critical failure mechanism when a terraced residence is subjected to the load combination in Fig. 1.
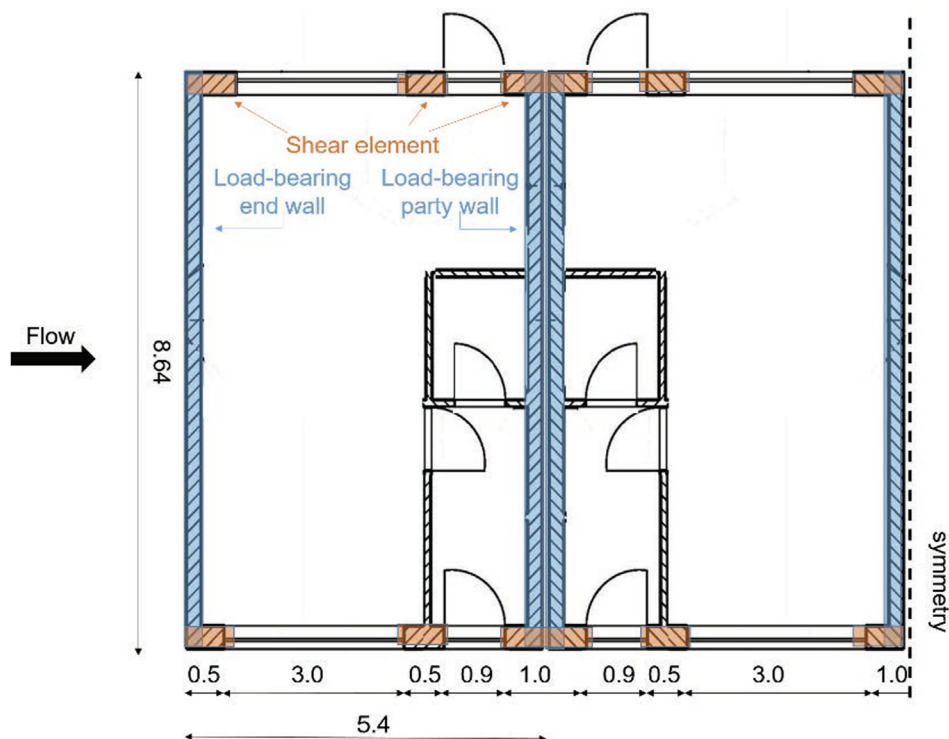

Fig. 11. Plan of a traditionally built corner and terraced house in a row of four residences. 2R depicted with symmetry for 4R.
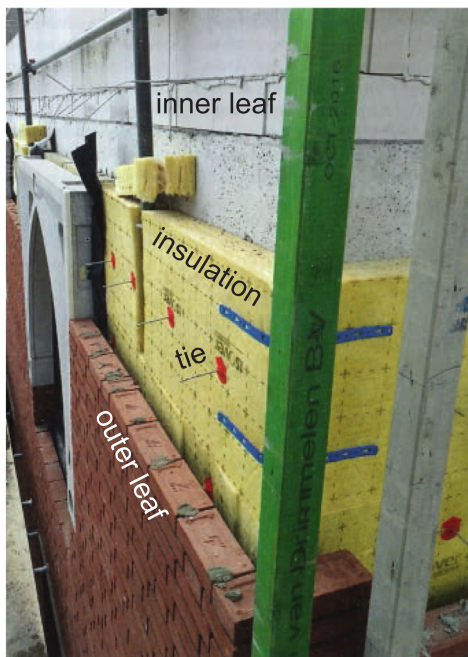
Fig. 12. Cavity wall [27]

4.2. Structural model of a load-bearing wall

It is assumed that the residence will collapse if the load-bearing inner leaf of the end-wall fails completely due to the flood actions in combination with the initial axial load applied from the floors and from the upper structure as determined in Table 3. Besides the dead load of the floor and wall, the inclined roof (e.g. timber gable roof or rafter roof) transfers its dead weight of approximately 0.75 kN/m^2 to the load-bearing walls resulting in an additional line load of 2.9 kN/m for a roof inclination of 45°. Furthermore, an additional surface load on the floors due to installations, furniture, etc. of 1 kN/m^2 is included. Since the vertical load has a favourable effect on the resistance of the wall, this load is multiplied with a factor γ of 0.9 in the analysis. The material properties defined from destructive laboratory tests on samples of existing buildings in the northern part of the Netherlands are used in combination with the material factors of 1.3 for masonry and 1.2 for concrete [6].

Looking at the boundary conditions of the walls from the case-study residences, the masonry walls are supported at all four edges: the wall is bonded to the piers in the façade which provides a clamped edge condition; then, due to the high normal force in the wall, the base of the wall in contact with the rigid foundation can be considered to be clamped, whereas the top is simply supported by the more flexible floor. However, in case of the concrete cast in-situ, the walls have a rigid connection with the floors, since the residences behave as a portal

Table 3
Properties of the load-bearing end wall for the three case-study residences.

Case-study residence	1	2	3
Material load-bearing walls	URM clay	URM calcium-silicate	URC C20/25
Thickness, t [mm]	100	120	120
Density, ρ [kg/m^3]	1800	1710	2400
Compression strength, f_k [MPa]	6.64	5.05	20
Flexural strength, f_{xk1} [MPa]	0.29	0.14	1.55
Material floors	Timber	System floor	RC
Weight, G [kN/m^2]	0.30 (+1)	5.40 (+1)	4.41 (+1)
Axial load on end wall, N_{Ed} [kN/m]	13.19	38.55	35.76

frame providing stability. Hence, a difference is made between the failure mechanism of the two-way bending behaviour in case of the masonry walls and the one-way bending behaviour of the concrete wall.

4.3. Failure mechanism of load-bearing wall

The axial load on top of the load-bearing wall due to the dead weight of the upper structure and the lateral load due to the hydrostatic and quasi-steady hydrodynamic component of the flood water causes bending stresses in the load-bearing wall. The magnitude of these loads, geometry of the walls and strength of the material determine in which stage of failure the wall will be. Fig. 13 depicts the following five different stages which can be distinguished during the process of failure of the wall.

Initially in Stage 0, the axial load on top of the load-bearing wall due to the dead weight of the upper structure is assumed to act in the middle of the wall, causing an initial compression stress which is distributed uniformly. If the lateral load is applied in Stage I, the compression stress increases at one side of the wall while decreasing at the other side of the wall until the tension strength of the material is reached. Since both unreinforced masonry and unreinforced concrete are weak in tension, a horizontal crack occurs at the tension side of the wall in Stage II. Increasing the load leads to opening of this first crack at the base of the wall until the stability moment or rocking strength is reached. Residual strength is obtained in Stage III due to the formation of multiple cracks in the horizontal direction (and diagonal direction in case of two-way bending) and redistribution of bending resistance along these cracks. For the collapse of the wall, the principle of virtual work is applied as in the Australian masonry code [13], so failure occurs in Stage IV when the external work, E_{ex}, is equal to the internal work, E_{in}, as described in Equation (6).

$$E_{ex} = E_{in} \text{ with} \begin{cases} E_{ex} = \sum \iint q(x,y) u_i(x,y) \, dx \, dy \\ E_{in} = \sum M_{Rd,i} l_i \theta_i \end{cases} \tag{6}$$

where 'q' describes the load, 'u' the out-of-plane displacement of the wall, 'M' the bending moment over a crack of length 'L', and 'θ' the work angle achieved by the moment; see [13] for details.

The post-cracking strength from rocking in Stage II and residual strength in Stage III is obtained by the development of the moments along the crack lines. For the one-way bending wall, the location of these horizontal cracks can be found from the locations where the highest moments occur during linear elastic deformation of the wall illustrated in Fig. 14a. For the two-way bending wall supported on all four sides, the crack pattern for uniformly loaded walls is obtained from various experiments. Only the contribution of the moments along the horizontal crack [26] and those along diagonal cracks in the direction of the natural slope (the angle of the crack, G_n, see [30]) are taken into account for the external work, since these are assumed to be fully developed simultaneously, while the vertical cracks are only partially developed [26]. Furthermore, due to the non-uniformly distributed hydraulic load, the location of the horizontal crack at mid-height in case of uniform load is assumed to shift downwards to the critical height, y_c, found from the one-way bending walls as pictured in Fig. 14. A uniform pressure would cause a horizontal crack at the middle of the height of the wall; the non-uniform pressure of the water, acting towards the bottom of the wall, shifts this crack downwards. Then, as a simplification, this lower position is assumed identical for the two-way bending and the one-way bending cases. In all cases, the height of the application of the resultant force from the hydraulic pressure is placed at the centroid of the pressure trapezoid.

4.4. Damage curves

The experimentally determined coefficients are used to translate the flood characteristics into a lateral load. This load deforms the load-
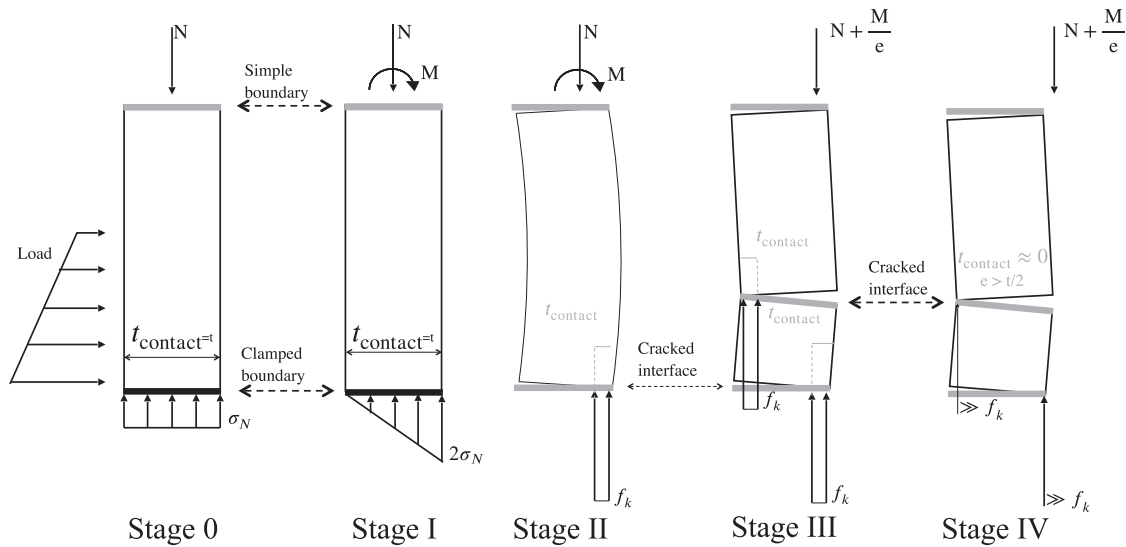
Fig. 13. Stresses along (cracked) cross sections of the load-bearing wall per stage.

bearing wall causing the different stages in the process of failure described in the previous section. Fig. 15 shows the flood combinations which lead to damage of the load-bearing wall for the three case-study residences. Here, the various lines delimit the stages at which the walls are expected to be due to a certain combination of water depth (hydrostatic, horizontal axis) and flow velocity (hydrodynamic, vertical axis), the latter are computed using the newly obtained pressure coefficients. The differences between the rocking strength (Stage II) of the case-study residences in Fig. 15 hint at the significant influence of the dead weight carried by the wall in combination with the compression strength and thickness of the wall on the capacity. Furthermore, the residual moment resistance (Stage III) of the masonry walls due to the two-way bending is quite large compared to those of the one-way bending concrete wall. These findings, as well as the shape of the curves, are in line with those of Kelman [9], who presents comparable load-bearing walls of British residences.

Despite the higher flexural bending strength, the resistance of the older residence with clay masonry walls and timber floors is smaller than those of the newer residences with calcium-silicate masonry walls and system floors or casted concrete walls and floors. This is mainly due to the formation of early cracks in the wall resulting in zero tensile strength after cracking and a higher normal force on the walls due to heavier system or concrete floors instead of timber floors. When the crack opens up, the eccentricity of this normal force causes residual moment capacity, which is substantially higher in the case of the newer residences. For Residence 1, a water depth of ~ 1.2 m already causes

the design moment resistance of the wall without taking the velocity into account. For the newer residences, Residence 2 and 3, this ultimate resistance is reached due to a water depth of ~ 1.8 m. If the flood water has a flow velocity of 2 m/s, the critical water depth reduces by ~ 0.3 m to respectively ~ 0.9 and 1.5 m.

In this paper, a simplification of the crack pattern (see Fig. 14) and a conservative design (reduced values of strength) are used to generate the damage functions in Fig. 15. These curves are all far below the Clausen criteria of h·v = 7 m²/s [1], thus indicating collapse before expected with the aforementioned criterion. However, this is in case of the most critical situation with the flow direction perpendicular to the load-bearing wall of the residence and no water inside the residence. Both a smaller angle of attack and water inside the residence will decrease the net load on the walls, resulting in higher water depths or flow velocities that can be resisted. To generate damage functions applicable to a total neighbourhood or city, the influence of a city-layout on the pressure and the flood infiltration rate are thus of great importance.

4.5. Sensitivity analysis

Due to the simplifications and conservative assumptions causing a potentially low capacity, two variations are addressed in a sensitivity analysis, namely:

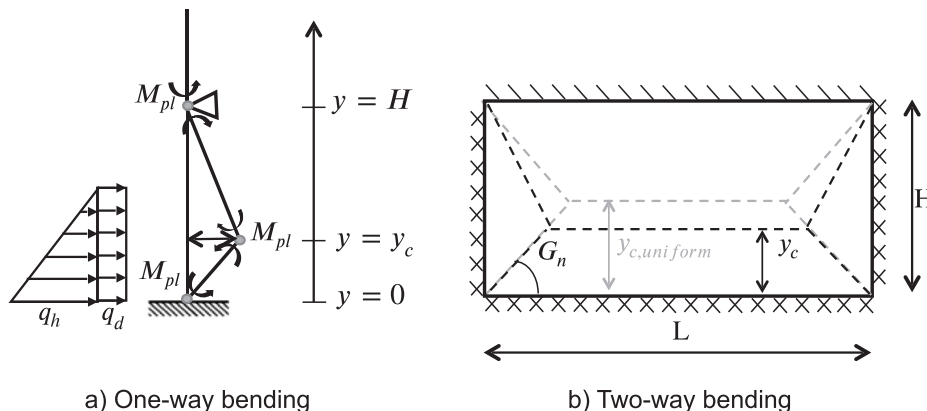the influence of dead weight carried by the wall in combination with

a) One-way bending b) Two-way bending

Fig. 14. Simplification of the crack patterns for walls due to the lateral flood load.
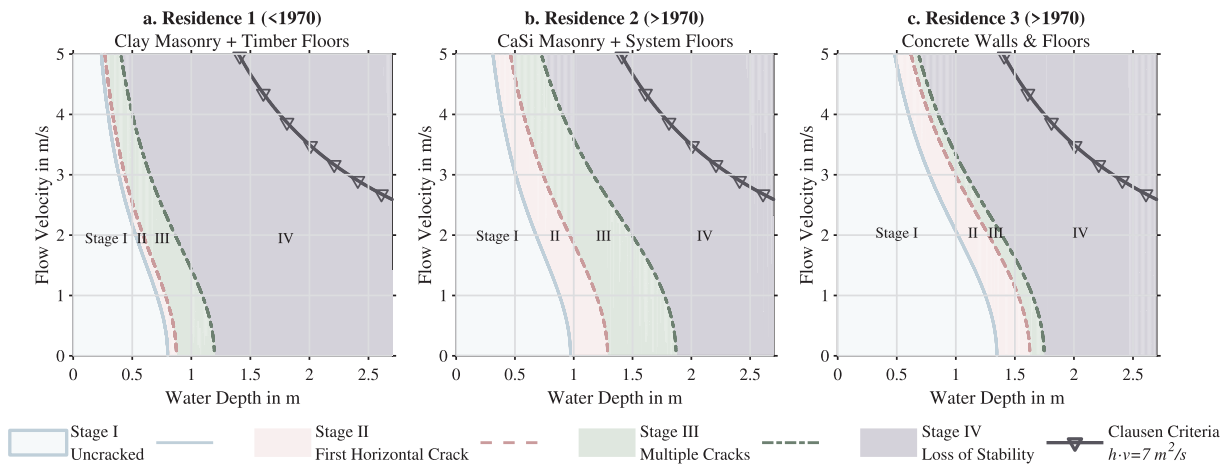
Fig. 15. Damage curves for three case-study residences.

the compression strength and thickness of the wall on the capacity; the water level difference between the inside and outside of the building.

The difference of the hydrostatic water pressure compared to the values from the previous section are discussed below. First, only the end walls of the row of terraced houses are subjected to the external flood load. For the traditionally built residences (clay masonry and timber floors), the load-bearing elements of the end- and party walls are identical, but for the concrete residences, the thickness of a massive unreinforced party wall is more than twice the thickness of the load-bearing leaf of the end wall to provide overall stability of the row of houses [29]. As the graph in Fig. 16a shows, both load-bearing walls of a terraced house (party walls) have a higher resistance than the end walls of the residence, which is one of the load-bearing walls of a corner house. The maximum water depth that the party wall can resist before collapse (Stage IV) is more than 70% higher than the water depth that the end wall can resist. Cracks occur at 50% of the ultimate water depth (Stage II) while the ultimate water depth itself would already be over the first-floor level. In Fig. 16a, the Clausen criteria matches well for the thicker party walls or for when the water depth inside the structure is equalised with the outside and the flow velocity is around 2.5 m/s. In

the latter case, the hydrostatic component of the flood does not play a role. For Residences 1 and 2 this increase in resistance due to the doubling of the wall thickness is significantly smaller, with an increase of resistance in terms of an additional water depth of respectively 40% and 55%. Doubling the initial stress on the wall instead of the thickness gives an additional water depth capacity of about 30% for all three case study residences. Considering these changes, the walls still collapse before the water depth reaches the first-floor level.

Similarly, the influence of the water level difference is investigated in Fig. 16b for Residence 2. In the previous section, the most extreme situation is taken into account with no water inside the residence, resulting in the black lines. However, if the rise rate of the flood is gradual, windows are open or broken or the infiltration rate is high, the water can easily enter the residence and rise until the water level is equalised. The shape of the damage curves changes especially for the lower flow velocities approaching a capacity of up to 2.5 m/s for when the water depth reaches the first-floor level; this critical velocity is about 1.5 m/s for Residence 1. Note that the pressure coefficients used to compute the forces have not been modified in this example; in reality, water entering the structures and flowing through the structure will lead to lower hydrodynamic pressure [32–34]; this reduction has been neglected. Nonetheless, it can be concluded that the true damage
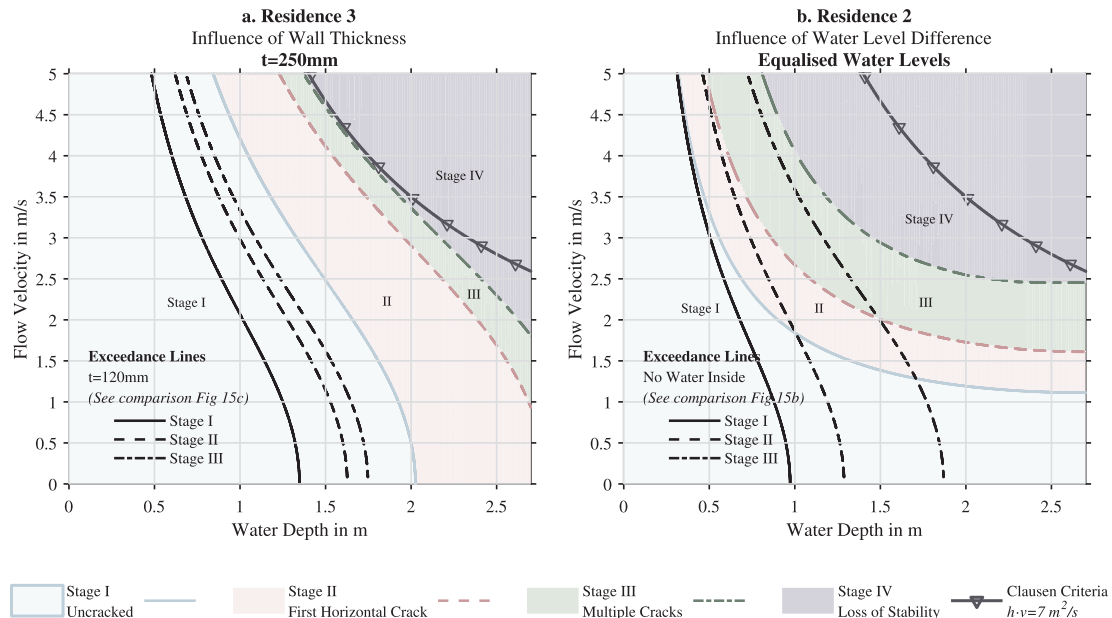

Fig. 16. Damage curves from sensitivity analysis (see Fig. 13 for definition of stages).

curves will lie somewhere in between the two most extreme cases of absolutely no water inside the structure and equalised water levels. Further study into the rise rate of the water inside and outside the residences is required.

5. Conclusions

This paper introduces the use of a pressure coefficient when defining the quasi-steady component of the hydrodynamic load on buildings due to flooding. Buildings reach collapse when a load-bearing wall fails, which is caused by pressure on this particular wall only, in a way similar as to when buildings are subjected to wind loading. The drag coefficient used currently defines the total force on the whole structure, and is thus only applicable for stiff structures and should not be used for analysing the collapse of individual walls. Higher drag coefficients (1.14 to 1.76) than those provided by FEMA [4] (1.2–1.3) are derived from experiments with a physical model of a rectangular box, resulting in higher hydrodynamic loads on the residences. However, the pressure coefficients on the frontal face of the residence are more in line with the values prescribed in the US guideline, but lower than those provided by the EuroCode for wind loading.

Furthermore, the current experiments have shown a positive dependence of both the width/water depth aspect ratio and the angle of attack on the pressure coefficient of the frontal face. For rectangular boxes with a small side ratio (length over width smaller than the inverse "Golden section" ratio of ~0.6 [16]) the pressure coefficient of the frontal face is significantly smaller than the drag coefficient; this is because the pressure on the rear face is negative; note that this concerns only the hydrodynamic pressure, as the hydrostatic pressure is almost equal on all sides when considering this form of parametrised hydrodynamic pressure. For higher ratios this difference is negligible.

The outcomes of this study show the importance of combined knowledge of hydraulic actions on, and structural damage of, residences in the current building stock to define the appropriate failure mechanism for each individual residence. To evaluate the capacity of the load-bearing walls in common Dutch terraced houses, the experimentally determined pressure coefficients are used to define the design load. The case study showed that these residences, when subjected to flow perpendicular to the load-bearing wall, reach collapse before the currently used damage functions indicate total failure. Yet, this is dependent on the water level inside the house, something that is not quantified in the empirical functions. Nevertheless, mitigation measures should be focussed on improving the resistance of the load-bearing walls in these cases by for example, increasing the thickness or placing an additional support halfway the length of the wall to decrease the span. Alternatively, the pressure of the incoming water could be decreased by increasing the rise rate inside the residence.

To derive damage functions for multiple geometries and orientations of the residences, more experiments defining the pressure coefficient could be helpful. On top of that, for the low flow velocities expected in most parts of the Netherlands, the sensitivity analyses show especially important influence of the flood infiltration rate inside the residence on the resistance of the wall. Since these damage functions are also used for the mortality functions, this physical approach will help better quantify the risk of loss of life as well.

Furthermore, additional research is needed to translate the local flood conditions at the building scale from larger scale models and newer higher resolution models. For the structural part of the research, it is recommended to extend the scenarios of multiple flood situations, such as the inclusion of the rise-rate inside the residence. A macro-scale approach is used in this study to analyse the failure of the wall, yet a more detailed approach is recommended to achieve accurate crack widths corresponding to specific damage stages in the fragility curves [11]. This could also benefit from the contribution of the tied outer leaf on the resistance of the cavity wall as a whole.

CRediT authorship contribution statement

L. Jansen: Conceptualization, Investigation, Formal analysis, Project administration, Writing - original draft, Methodology. **P.A. Korswagen:** Writing - review & editing, Visualization, Conceptualization, Methodology. **J.D. Bricker:** Conceptualization, Supervision, Writing - review & editing, Funding acquisition. **S. Pasterkamp:** Supervision, Writing - review & editing, Methodology. **K.M. Bruijn:** Supervision, Writing - review & editing. **S.N. Jonkman:** Supervision, Writing - review & editing.

Declaration of Competing Interest

The authors declare that they have no known competing financial interests or personal relationships that could have appeared to influence the work reported in this paper.

Appendix A. Supplementary material

Supplementary data to this article can be found online at https://doi.org/10.1016/j.engstruct.2020.110647.

References

[1] Clausen, L., and P. B. Clark. "The development of criteria for predicting dambreak flood damages using modelling of historical dam failures." International conference on river flood hydraulics. John Wiley & Sons Ltd. Hydraulics Research Limited, Wallingford, England; 1990.

[2] Chen X, Jonkman S, Pasterkamp S, Suzuki T, Altomare C. Vulnerability of buildings on coastal dikes due to wave overtopping. Water 2017;9(6).

[3] De Bruijn K, van Kester B. Possibilities to improve flood fatality functions for the Netherlands. Delft, The Netherlands: Deltares; 2015.

[4] FEMA. Coastal construction manual: Principles and practices of planning, siting, designing, constructing, and maintaining residential buildings in coastal areas. FEMA 2011. P-55.

[5] Foster ASJ, Rossetto T, Allsop W. An experimentally validated approach for evaluating tsunami inundation forces on rectangular buildings. Coast Eng 2017;128:44–57.

[6] Jafari S, Rots JG, Esposito R, Messali F. Characterizing the material properties of Dutch unreinforced masonry. Procedia Eng 2017;193:250–7.

[7] Jansen L. Structural damage to Dutch terraced houses due to flood actions. Delft, The Netherlands: Delft University of Technology; 2019.

[8] Jonkman, S.N. "Loss of life estimation in flood risk assessment; theory and applications." PhD thesis, Delft University of Technology, Delft, The Netherlands; 2007.

[9] Kelman I. Physical flood vulnerability of residential properties in coastal, eastern England. Diss: University of Cambridge; 2002.

[10] Kelman I, Spence R. An overview of flood actions on buildings. Eng Geol 2004;73(3–4):297–309.

[11] Korswagen PA, Jonkman Sebastiaan N, Terwel KC. Probabilistic assessment of structural damage from coupled multi-hazards. Struct Saf 2019;76:135–48.

[12] Lauber G, Hager WH. Experiments to dambreak wave: Horizontal channel. J Hydraul Res 1998;36(3):291–307.

[13] Lawrence S, Marshall R. Virtual work design method for masonry panels under lateral load. 12 th Int Brick/Block Masonry Conf Proc 2000;2:1063–73.

[14] Maaskant B, Jonkman SN, Kok M. "Analyse slachtofferaantallen VNK-2 en voorstellen voor aanpassingen van slachtofferfuncties". Rapport PR1669(10). HKV Lijn. Water 2009 (in Dutch).

[15] Nakaguchi H. An experimental study on aerodynamic drag of rectangular cylinders. J. JSASS 1968;16:1–5.

[16] Norberg C. Flow around rectangular cylinders: pressure forces and wake frequencies. J Wind Eng Ind Aerodyn 1993;49(1–3):187–96.

[17] Pistrika AK, Jonkman SN. Damage to residential buildings due to flooding of New Orleans after hurricane Katrina. Nat Hazards 2010;54(2):413–34.

[18] Rietmeijer A. Rear-Slope Revetment Stability Approached by the Wave Overtopping Simulator. Delft, The Netherlands: Delft University of Technology; 2017.

[19] Rijkswaterstaat. Over overstroomik?, 2019. https://overstroomik.nl/ over-overstroomik.html.

[20] Ritter A. Die fortpflanzung der wasserwellen. Zeitschrift des Vereines Deutscher Ingenieure 1892;36(33):947–54.

[21] Roos, W. "Damage to buildings." Delft Cluster report DC1-233-9; 2003.

[22] Slager K, Wagenaar D. Standaardmethode 2017: schade en slachtoffers als gevolg van overstromingen. Delft, The Netherlands: Deltares; 2017 (in Dutch).

[23] Slager K De. ramp: een reconstructie: 200 ooggetuigen over de watersnood van 1953 verhalen om nooit om vergeten. De Koperen Tuin 1992 (in Dutch).

[24] Thijssen CCF. Bouwconstructieve analyse van naoorlogse eengezinshuizen in de non-profit huursector 1946–1980. Delft University Press; 1999.

[25] Tennakoon KBM. Parameterisation of 2D hydrodynamic models and flood hazard mapping for Naga city, Philippines. Enschede: ITC; 2004.

[26] Vaculik J, Griffith MC. Out-of-plane load–displacement model for two-way spanning masonry walls. Eng Struct 2017;141:328–43.

[27] Van Wijlick S, Vekemans H. Nut en noodzaak belicht: Wel of geen geventileerde spouwmuur? De Aannemer 2018 (in Dutch).

[28] Vischer, D. L., & Hager, W. H. "Dam hydraulics." John Wiley & Sons, Chichester, West Sussex PO 19 1 UD(UK). 316; 1998.

[29] VOBN, "Construeren van gietbouwcasco's" Veenendaal; 2003. (in Dutch).

[30] Willis C. Design of unreinforced masonry walls for out-of-plane loading PhD Thesis University of Adelaide, Australia; 2004.

[31] Wüthrich D, Pfister M, Nistor I, Schleiss AJ. Experimental study of tsunami-like waves generated with a vertical release technique on dry and wet beds. J Waterw Port Coastal Ocean Eng 2018;144(4):04018006.

[32] Triatmadja R, Nurhasanah A. Tsunami force on buildings with openings and protection. J Earthq tsunami 2012;6(4):1250024.

[33] Hartana K, Murakami. Numerical and experimental simulation of two-phase tsunami flow through buildings with openings. J Earthq Tsunami 2015;9(3):1550007.

[34] Wüthrich D, Pfister M, Nistor I, Schleiss AJ. Experimental study on forces exerted on buildings with openings due to extreme hydrodynamic events. Coast Eng 2018;140:72–86.

[35] Gupta VP, Goyal SC. Hydrodynamic Forces on Bridge Piers. J Inst Engineers (India) 1975;56:12–6.

[36] Arnason H, Petroff C, Yeh H. Tsunami bore impingement onto a vertical column. J Disaster Res 2009;4(6):391–403. https://doi.org/10.20965/jdr.2009. p0391.

[37] Wüthrich D, Pfister M, Nistor I, Schleiss AJ. Experimental study on the hydrodynamic impact of tsunami-like waves against impervious free-standing buildings. Coastal Eng J 2018;60(2):180–99.

[38] Peakall J, Warburton J. Surface tension in small hydraulic river models-the significance of the weber number pages 199??212 J Hydrology (New Zealand)1996.

[39] Shafiei S, Melville BW, Shamseldin AY. Experimental Investigation of Tsunami Bore Impact Force and Pressure on a Square Prism. Coast Eng 2016;110:1–16.

[40] Wind, H.G., Nierop, T.M., de Blois, C.J. & de Kok, J.L. (1999). Analysis of flood damages from the 1993 and 1995 Meuse floods. Water Resources Research, Vol 35, No 11, Pages 3459-3465, November 1999.

[41] Nistor, I., Palermo, D., Nouri, Y., Murty, T. & Saatcioglu, M. (2008). Tsunami-Induced Forces on Structures. Department of Civil Engineering, University of Ottawa.

[42] Nouri, Y., Nistor, I. & Palermo, D. (2010). Experimental Investigation Of Tsunami Impact On Free Standing Structures. Coastal Eng J, Vol. 52, No. 1 (2010) 43-70.